

Hybrid quantum-classical unsupervised data clustering based on the Self-Organizing Feature Map

I. D. Lazarev

*Federal Research Center of Problems of Chemical Physics and Medicinal Chemistry RAS,
Chernogolovka, Moscow Region, Russia, 142432 and
Faculty of Fundamental Physical-Chemical Engineering,
Lomonosov Moscow State University, GSP-1, Moscow, Russia 119991*

Marek Narozniak

*New York University Shanghai, 567 West Yangsi Road, Shanghai, 200122, China.
Department of Physics, New York University, New York, NY, 10003, USA. and
sqrtxx.com, Krakowiaków 4, 20-255, Warsaw, Poland*

Tim Byrnes

*New York University Shanghai, 567 West Yangsi Road, Shanghai, 200126, China.
NYU-ECNU Institute of Physics at NYU Shanghai,
567 West Yangsi Road, Shanghai, 200126, China.
Shanghai Frontiers Science Center of Artificial Intelligence and Deep Learning,
567 West Yangsi Road, Shanghai, 200126, China.
State Key Laboratory of Precision Spectroscopy, School of Physical and Material Sciences,
East China Normal University, Shanghai 200062, China
Center for Quantum and Topological Systems (CQTS),
NYUAD Research Institute, New York University Abu Dhabi, UAE. and
Department of Physics, New York University, New York, NY 10003, USA*

A. N. Pyrkov*

*Federal Research Center of Problems of Chemical Physics and Medicinal
Chemistry RAS, Chernogolovka, Moscow Region, Russia, 142432
(Dated: July 29, 2023)*

Unsupervised machine learning is one of the main techniques employed in artificial intelligence. Quantum computers offer opportunities to speed up such machine learning techniques. Here, we introduce an algorithm for quantum assisted unsupervised data clustering using the self-organizing feature map, a type of artificial neural network. We make a proof-of-concept realization of one of the central components on the IBM Q Experience and show that it allows us to reduce the number of calculations in a number of clusters. We compare the results with the classical algorithm on a toy example of unsupervised text clustering.

I. INTRODUCTION

The combination of big data and artificial intelligence — dubbed the fourth industrial revolution — has profoundly affected the modern economy in a plethora of different ways from robotics to agriculture [1–5]. Contemporary artificial intelligence methods based on neural networks also have the potential to enhance the role of novel analytical methods in science and engineering [6–8]. Paradoxically, the intrinsic mechanism of how neural networks work and why they are so powerful remains unknown (in many cases it is regarded as a black box). It has been speculated that limits to the neural network paradigm based on the computational power of von Neumann architecture are being approached, and improvements appear only due to heuristic escalation of complexity [9–11].

In particular, the self-organizing feature map (SOFM) [12–14], is a type of artificial neural network (ANN) that is trained in an unsupervised manner. SOFMs are used in many areas [15–22] and in comparison with many other artificial neural networks, they apply competitive learning and preserve the topological properties of the input space [23]. The SOFMs represent data in a fundamentally topological way that allows one to perform dimensionality reduction. Once it is trained, the map can classify a vector from the input space by finding the node with the smallest distance metric.

Meanwhile, there has been much interest recently in applying quantum computing techniques to machine learning [24–27]. The main focus of early works in quantum machine learning (QML) was in obtaining a quantum speedup [25, 26] by applying quantum approaches to solve linear algebra problems, such as the Fourier transform or solving systems of linear equations [28–30]. Quantum algorithms were developed for linear regression, principal component analysis, support vector machine, K-means algorithm and others [31–35]. More recently,

* Email address:pyrkov@icp.ac.ru

there has been attention on developing quantum neural networks [36–39]. The interest in quantum neural networks was inspired by progress in experimental quantum computing when it became possible to use parametrized quantum circuits, where the parameters behave much like the weights of a neural network [40]. In particular, quantum algorithms for training and evaluating feedforward neural networks were developed, which are one of the most usable neural network models [41, 42]. Quantum models for convolutional neural networks, which may be suitable for the problems of learning of quantum states were also proposed [43, 44]. Recent results connecting the classical Bayesian approach to deep learning allowed for the development of a new algorithm for Bayesian deep learning on quantum computers [45]. For the problem of classification which is closely connected to the problem of clusterization, a protocol of quantum classification, tested on the MNIST dataset, via slow feature analysis based on the use of quantum Frobenius distance was proposed [46]. Furthermore, many other hybrid and quantum protocols inspired classical neural networks were developed [47–61].

At the same time, non-neural-network based hybrid quantum classical algorithms have become a new direction of significant interest [62–64]. Such hybrid algorithms involve quantum circuits used for part of the execution and is typically trained in a classical learning loop. In particular, the Quantum Approximate Optimization Algorithm (QAOA) was developed to find approximate solutions to combinatorial optimization problems [65, 66] and designed for problems such as MAX-CUT and Grover’s algorithm [63, 64, 67–72]. Another example of a well-known hybrid quantum classical algorithm is the Variational Quantum Eigensolver (VQE) for applications in quantum simulations [73–76]. Currently, it is believed that implementation of quantum neural networks and hybrid quantum classical algorithms can be the main test bed to achieve practical quantum supremacy on Noisy Intermediate Scale Quantum (NISQ) devices [77].

In this paper, we develop a hybrid quantum-assisted SOFM (QASOFM) and apply it to the data clustering problem in an unsupervised manner. The idea is based on the use of the Hamming distance as a distance metric for the training the SOFM that allows, in the quantum case, to reduce the number of distance calculations in the number of clusters and thus to speed up the original classical protocol. In order to make our protocol more appropriate for the currently available generation of NISQ quantum devices, we optimized a circuit for realizing the Hamming distance by reducing number of one-qubit operations. We then apply it to a toy example of clustering paper abstracts and give a proof-of-concept realization of the quantum assisted SOFM on the IBM Q experience quantum computer [78] and compare it to the classical case.

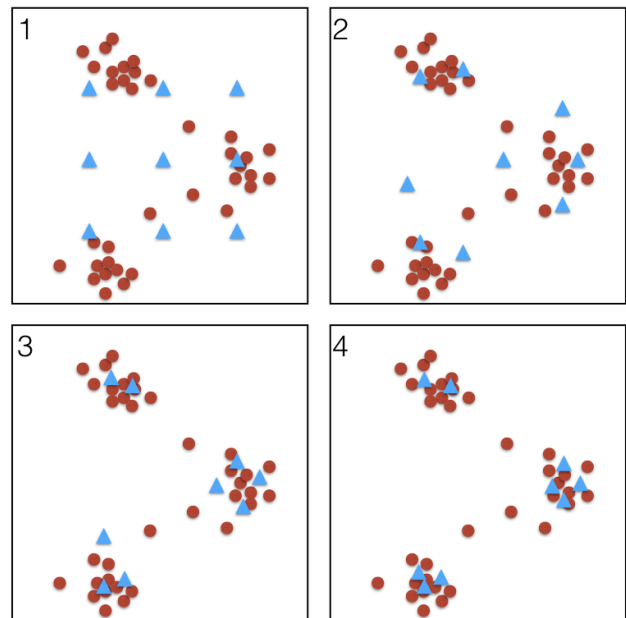


FIG. 1. Schematic illustration of the clustering problem considered in this paper. Blue triangles represent clusters and red circles are data points. The training process moves clusters to fit the data points. Note that there are fewer clusters than data points, which is the essence of dimensionality reduction, and is what permits the model to generalize the data.

II. THE QUANTUM ASSISTED SELF-ORGANIZING FEATURE MAP (QASOFM)

A. The classical algorithm

The SOFM is one of the most widely-used unsupervised learning methods used in various areas of modern science. It was first proposed by Kohonen as a self-organizing unsupervised learning algorithm which produces feature maps similar to those occurring in the brain [79]. The SOFM algorithm operates with a set of input objects, each represented by a N -dimensional vector, and describes a mapping from a higher-dimensional input space to a lower-dimensional map space that preserves the topological properties of the input space, commonly referred to as a bi-dimensional map.

The input dimensions are associated with the features, and the nodes in the grid (called cluster vectors) are assigned the N -dimensional vectors. The components of these vectors are usually called weights. Initially the weight components are chosen randomly. The SOFM is then trained by adjusting the components through the learning process which occur in the two basic procedures of selecting a winning cluster vector, also called the best matching unit (BMU), and updating its weights (Fig. 1). More specifically, they consist of the four step process: 1. select an input vector randomly from the set of all input vectors; 2. find a cluster vector which is closest to the input vector; 3. adjust the weights of the best matching

unit and neurons close to it on the feature map in such a way that these vectors becomes closer to the input vector; 4. repeat this process for many iterations until it converges.

On a step t when the best matching unit \vec{w}_c for a input $\vec{x}(t)$ is selected, the weights \vec{w}_i of the best matching unit and its neighbors on the feature map are adjusted according to

$$\vec{w}_i(t+1) = \vec{w}_i(t) + \theta(c, i, t) \alpha(t) (\vec{x}(t) - \vec{w}_i(t)). \quad (1)$$

Here, $\alpha(t)$ is the monotonically decreasing learning rate and $\theta(c, i, t)$ is the neighborhood function (usually taken as a Gaussian or delta function) which defines the vicinity of the BMU labeled by an index c , the weights of the neighbors in the vicinity should also be adjusted in the same manner as for the BMU. This expression can be understood in the following way: if a component of the input vector $\vec{x}(t)$ is greater than the corresponding weight $\vec{w}_i(t)$, increase the weight of the BMU and the weights indexed by i and defined with the neighborhood function by a small amount defined by the learning rate $\alpha(t)$; if the input component is smaller than the weight, decrease the weight by a small amount. The larger the difference between the input component and the weight component, the larger the increment or decrement.

Intuitively, this procedure can be geometrically interpreted as iteratively moving the cluster vectors defined by the corresponding weight $\vec{w}_i(t)$ (blue triangles on Fig. 1) in space one at a time in a way that ensures each move is following the current trends inferred from their distances to the input objects defined by $\vec{x}(t)$ (red circles on Fig. 1).

In the original version of SOFM, the winning cluster vector is selected based on the Euclidean distance between an input vector and the cluster vectors. In this paper, we deal with a binary vector clustering problem, where the Hamming distance is more suitable [80, 81]. Using a simple technique of encoding classical binary information into a quantum register [82], we introduce an optimized algorithm for calculating the matrix of Hamming distances between all input and cluster vectors at once.

B. Optimized quantum scheme for Hamming distance calculation

The overall procedure involves two registers of n qubits each, denoted $|X\rangle$ and $|Y\rangle$, along with a single auxiliary qubit $|a\rangle$. During the whole process, the $|Y\rangle$ register is used to store the cluster states. At the beginning and end of the procedure, the $|X\rangle$ register stores the input vectors. During the procedure it stores the differences between input vectors and cluster states.

Let us assume we have N_x input vectors and N_y cluster states. The i th input vector and j th cluster vector are respectively denoted as $|x_i\rangle$, $|y_j\rangle$. The registers $|X\rangle$ and $|Y\rangle$ are initialized to store the input vectors and cluster

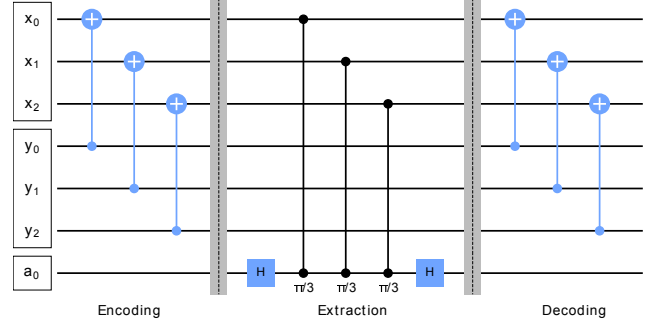


FIG. 2. Quantum circuit for the quantum parallelized Hamming distance calculation between all pairs of binary vectors from two sets X and Y . First, we encode information about pairwise different qubits in a quantum state of the X -register by applying the CNOT gates. Second, the Hamming distance values are extracted to the amplitudes of superposition with the control phase rotation (see Eq. (6)) and Hadamard gates. Finally, a quantum space of the X -register is returned to the initial basis for information retrieval.

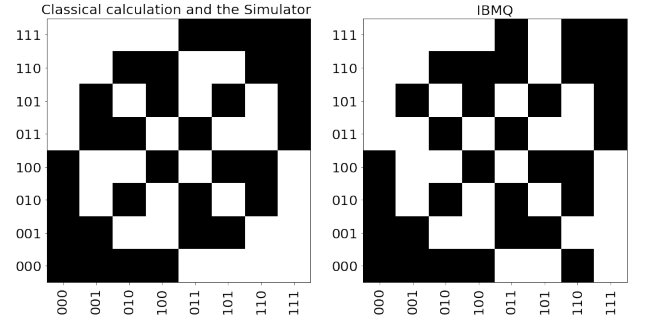


FIG. 3. Hamming distance matrix between two data sets of binary vectors. Values of distance that less than median distance value was marked black. The classical simulation of the quantum circuit shows perfect agreement to theoretical calculations and presented on the left figure. Result obtained on IBMQ “ibmq_16_melbourne” backend is shown on the right figure and the accuracy in comparison with the classical simulation is more than 92 %.

vectors according to

$$|X\rangle = \frac{1}{\sqrt{N_x}} \sum_{i=1}^{N_x} |x_i\rangle, \quad (2)$$

$$|Y\rangle = \frac{1}{\sqrt{N_y}} \sum_{j=1}^{N_y} |y_j\rangle. \quad (3)$$

The two registers along with the auxiliary qubit comprise the initial state of the quantum computer according to

$$|\psi_0\rangle = |X\rangle |Y\rangle |0\rangle. \quad (4)$$

Given this initial state we may begin the processing of the problem. The quantum circuit that we follow is shown in Fig.2. We start by elementwise applying CNOT

gates between all the qubits of the X and Y registers (the “Encoding” part of Fig. 2)

$$|\psi_1\rangle = \frac{1}{\sqrt{N_x N_y}} \sum_{i,j=1}^{N_x, N_y} |d_{ij}^{(1)}, \dots, d_{ij}^{(n)}\rangle |y_j^{(1)}, \dots, y_j^{(n)}\rangle |0\rangle, \quad (5)$$

where $d_{ij}^{(\alpha)} = \text{CNOT}(y_i^{(\alpha)}, x_j^{(\alpha)})$, and $\alpha = 1 \dots n$ is the qubit index in the register. At this stage of the computation the $|X\rangle$ no longer stores the input vectors, instead it stores the information about pairwise different qubits between the input vectors $|x_i\rangle$ and cluster vector $|y_j\rangle$.

The next step, depicted on the Fig.2 as the “Extraction” stage, is to extract the accumulated information about the differences between each pair $|x_i\rangle$ and $|y_j\rangle$ by projection onto the amplitude of the superposed state. This is achieved by applying the Hadamard gate on the auxiliary qubit, followed by a controlled phase gate on $|a\rangle |d_{ij}^{(\alpha)}\rangle$, where the phase gate is defined by

$$R_{(X,a)}(\phi) = \begin{pmatrix} 1 & 0 & 0 & 0 \\ 0 & 1 & 0 & 0 \\ 0 & 0 & 1 & 0 \\ 0 & 0 & 0 & e^{-i\phi} \end{pmatrix}, \quad \phi = \frac{\pi}{n} \quad (6)$$

where $d_{ij}^{(\alpha)}$ is the control qubit and the ancilla qubit $|a\rangle$ is the target. Finally, another Hadamard gate is applied on the ancilla qubit (see Fig. 2).

After the first Hadamard on the ancilla qubit the state is

$$|\psi_2\rangle = \frac{1}{\sqrt{N_x N_y}} \sum_{i,j=1}^{N_x, N_y} |d_{ij}\rangle |y_j\rangle \frac{(|0\rangle + |1\rangle)}{\sqrt{2}}, \quad (7)$$

where $|d_{ij}\rangle = |d_{ij}^{(1)}, \dots, d_{ij}^{(n)}\rangle$. Applying the controlled phase gate on $|x^{(\alpha)}a\rangle$, where $\alpha = 1 \dots n$ the state then becomes

$$\begin{aligned} |\psi_3\rangle &= R_{(X,a)}\left(\frac{\pi}{n}\right) |\psi_2\rangle = \frac{1}{\sqrt{2N_x N_y}} \sum_{i,j=1}^{N_x, N_y} |d_{ij}\rangle |y_j\rangle |0\rangle \\ &+ \frac{1}{\sqrt{2N_x N_y}} \sum_{i,j=1}^{N_x, N_y} \exp\left(\frac{-i\pi}{n} \sum_{l=1}^n d_{ij}^{(l)}\right) |d_{ij}\rangle |y_j\rangle |1\rangle. \end{aligned} \quad (8)$$

Applying another Hadamard on the ancilla qubit we obtain

$$\begin{aligned} |\psi_4\rangle &= \frac{1}{\sqrt{N_x N_y}} \sum_{i,j=1}^{N_x, N_y} \exp\left(\frac{-i\pi}{2n} \sum_{l=1}^n d_{ij}^{(l)}\right) \\ &\times \left[\cos\left(\frac{\pi}{2n} \sum_{l=1}^n d_{ij}^{(l)}\right) |d_{ij}\rangle |y_j\rangle |0\rangle \right. \\ &\left. + i \sin\left(\frac{\pi}{2n} \sum_{l=1}^n d_{ij}^{(l)}\right) |d_{ij}\rangle |y_j\rangle |1\rangle \right]. \end{aligned} \quad (9)$$

This completes the step of projecting differences between pairs of $|x_i\rangle$ and $|y_j\rangle$ onto the amplitude of the auxiliary qubit. The process is done in the x -basis, achieved by the surrounding Hadamard gates. There are two possible measurement outcomes of the auxiliary qubit. Each pair of $|x_i\rangle$ and $|y_j\rangle$ forms a subspace of the Hilbert space, the controlled phase gate ensures to change amplitudes of those outcomes within this subspace depending on how different the spin configurations between $|x_i\rangle$ and $|y_j\rangle$ are.

At this stage, the information regarding the differences between pairs of $|x_i\rangle$ and $|y_j\rangle$ is encoded in the amplitudes. In order to extract the Hamming distances between the relevant $|x_i\rangle, |y_j\rangle$ we return to our initial basis for register $|X\rangle$ by applying pairwise CNOT gates:

$$\begin{aligned} |\psi_f\rangle &= \text{CNOT}(Y, X) |\psi_4\rangle \\ &= \sum_{i,j=1}^{N_x, N_y} \exp\left(\frac{-i\pi}{2n} \sum_{l=1}^n d_{ij}^{(l)}\right) \left[\cos\left(\frac{\pi}{2n} \sum_{l=1}^n d_{ij}^{(l)}\right) |x_i\rangle |y_j\rangle |0\rangle \right. \\ &\quad \left. + i \sin\left(\frac{\pi}{2n} \sum_{l=1}^n d_{ij}^{(l)}\right) |x_i\rangle |y_j\rangle |1\rangle \right]. \end{aligned} \quad (10)$$

Thus we return into the initial basis and the amplitudes of the auxiliary qubit are proportional to how different each pairs of $|x_i\rangle$ and $|y_j\rangle$ are.

From the statistics of the measurement outcomes of the final state (10) we recreate the amplitudes of ancilla qubit states. From those amplitudes estimations we are able to plot the distance matrix between two data sets of binary vectors. The probability amplitude of the ancilla qubit outcomes captures the exact Hamming distance as the result of the preprocessing function. There are two possible outcomes of measurement of the ancilla qubit, each has its probability amplitude and own interpretation of that amplitude. For instance, for the $|0\rangle$ outcome, the larger the amplitude the smaller the Hamming distance, and for the $|1\rangle$ outcome it is the other way around, the magnitude of the amplitude of that outcome is proportional to the Hamming distance.

Measuring the Hamming distance of a particular pair of input vectors $|x_i\rangle$ and cluster vectors $|y_j\rangle$ consists of extracting the relevant amplitude from the subspace that those states form, this can be done using the following projection operator

$$\Pi_{i,j} = |x_i\rangle\langle x_i| \otimes |y_j\rangle\langle y_j| \otimes I. \quad (11)$$

Using the above projection operator, the subspace of the Hilbert space formed by a particular pair of input and cluster vectors can be traced out as

$$\rho_{i,j} = \text{Tr}_{X,Y}(\Pi_{i,j} |\psi_f\rangle\langle\psi_f| \Pi_{i,j}). \quad (12)$$

From the reduced density matrix, the following two amplitudes for the measurement results can be extracted

$$a_0(x_i, y_j) = \frac{\langle 0 | \rho_{i,j} | 0 \rangle}{\text{Tr}(\rho_{i,j})} \quad (13)$$

$$a_1(x_i, y_j) = \frac{\langle 1 | \rho_{i,j} | 1 \rangle}{\text{Tr}(\rho_{i,j})}. \quad (14)$$

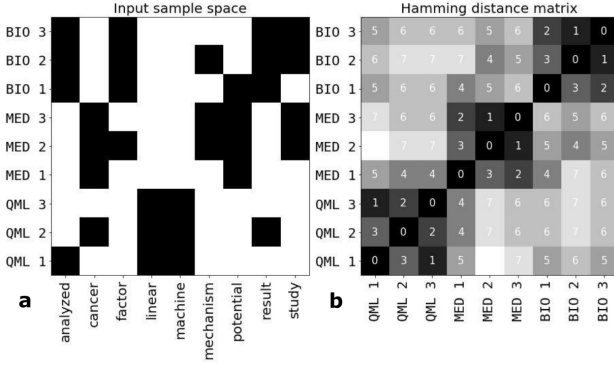


FIG. 4. (a) Representation of the data set of abstracts with the bag-of-words [83] model is shown. Each abstract is represented by a binary vector with 9 elements, corresponding to the 9 words on the horizontal axis. The samples are sorted into groups “Quantum Machine Learning” (QML), “Cancer” (MED) and “Gene Expression” (BIO) with 3 papers for each tag, for a total of 9 paper. (b) The Hamming distance between each vectorized abstract is shown as a number in the matrix.

Currently available quantum platforms are still subject to a substantial level of noise and extracting the exact distance from amplitude is still a difficult task. In order to reduce noise we average the measurement results over different states of the ancillary qubit, thus the measured Hamming distance between the input vector $|x_i\rangle$ and cluster vector $|y_j\rangle$ is

$$d_{i,j}^H \propto 1 - \frac{1}{2}(a_0(x_i, y_j) + (1 - a_1(x_i, y_j))). \quad (15)$$

The Hamming distance measured in this way is bounded $0 \leq d_{i,j}^H \leq 1$, where 0 indicates that x_i and y_j are identical and 1 means they are the completely opposite in terms of their pairwise binary coordinates.

The number of controlled gate operations to define the full distance matrix matches the number of controlled gate operations in Ref. [82], where the original algorithm for calculation of the Hamming distance was introduced, but the number of remaining gates is reduced compared to Ref. [82], leading to a less deep circuit, which is significant for NISQ devices.

III. EXPERIMENTAL DEMONSTRATION OF QASOFM

We now show experimental results for a proof-of-concept demonstration of the algorithm introduced in the previous section, on a 16-qubit quantum computer provided by IBM Q Experience. We perform unsupervised data clustering for three sets of paper abstracts from three different fields: quantum physics [84–86], medicine [87–89] and biology [90–92]. Each set consists of three papers selected at random that focus on one of the following topics: “Quantum Machine Learning”, “Cancer” and “Gene Expression”. Abstracts were vectorized by the

bag-of-words [83] model in order to choose the most defining words in each data set (see Fig. 4) [93]. This model represents text as a multiset “bag” of its words taking into account only the multiplicity of words. Preparing the bag-of-words we excluded the words that appear only in one abstract and more than in 4 abstracts and we also excluded the word “level” from consideration due to the frequent overlap between the clusters because it gives instabilities for both classical and quantum algorithms. We restricted our bag-of-word size to 9 of the most frequent words from the full bags-of-word due to limitations on the number of qubits. After vectorizing and pre-processing the data, the clusters are well-separated with the Hamming distance. We observe that distances between the abstracts inside clusters are smaller than distances between the abstracts from different clusters, showing successful self-organization (Fig. 4).

In classical SOFM [12], first a distance calculation between a sample vector and all cluster vectors is made, then the closest cluster vector is shifted towards the sample vector. The complexity of algorithm, in the sense of the number of distance calculations, scales as $O(LMN)$, where N is number of samples, M is number of randomly sampled cluster vectors, and L is number of the shifts of cluster vectors. In the QASOFM described in the previous section, distance calculations are realized on a quantum device (i.e. the IBM Q Experience) with the use of circuit presented in Fig. 2. This approach allows one to reduce the number of operations in a number of cluster states with an optimized number of gates that are possible to realize on quantum computing devices that are currently available. The calculation of Hamming distance implemented step-by-step between each sample vector and all cluster vectors is realized in one operation. In this case, as there is only one input vector considered, the “Decoding” stage (Fig. 2) can be removed as the measurement no longer needs to indicate for which input vector the distance has been measured. The complexity of the quantum assisted SOFM then scales as $O(LN)$.

In order to check that our algorithm gives the expected results we compare it to classical calculations of the distance matrix on two data sets of binary vectors, as shown in Fig. 3. We see good agreement between the distance matrices calculated classically and on the IBM Q Experience. The match is close, but not perfect, and we attribute it to noise in the currently available non fault-tolerant quantum processors.

An example of the QASOFM learning process is shown in Fig. 5. Initially, the cluster vectors were randomly chosen and the label of sample distribution is shown for the zeroth epoch in Fig. 5(a). In order to prepare a superposition of cluster vectors needed for the calculation of the distance matrix we use the standard initialization of QISKIT[94] library. Each epoch of the algorithm consists of distance calculation between all data and cluster vectors and requires 9 distance calculations in the quantum implementation (N in general case) or 27 distance calculations for classical realization (MN in general case).

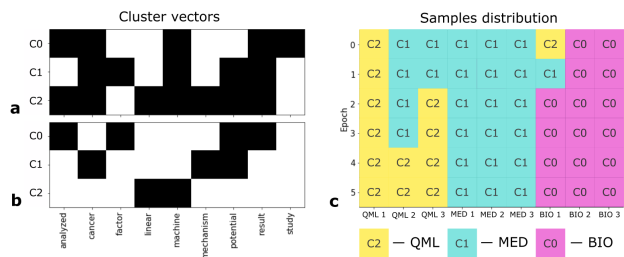


FIG. 5. (a) Initial random binary vectors of cluster vectors (labeled as C0, C1, C2), for the selected 9 words from the bag of words model. (b) The result of applying our QASOFM implemented on the IBM Q Experience simulator backend. Vectors mean cluster elements for BIO, MED, QML groups, for the C0, C1, C2 cluster vectors, respectively. (c) The evolution of label distribution on each learning epoch.

After the distance calculation from each sample to all cluster vectors at each epoch we label each sample with the index of the closest cluster vector and shift the closest cluster vectors to the sample vectors. The shift is made by the change of the first binary element in the cluster vectors which does not match the binary element in the sample vector. The evolution of the labels presented on Fig. 5(c). Good convergence is already observed in the fourth epoch.

This proof of concept example shows that the development of noisy intermediate scale quantum hardware will allow to solve some practical problems in unsupervised manner with a very simple encoding of categorical data to the quantum register. Furthermore, it shows that it is possible to develop distance based hybrid quantum classical algorithms that speed up classical counterparts and can be implemented on near-term quantum devices developing distance based hybrid algorithms. Such algorithms, that can learn in an unsupervised manner, for categorical data such as genomic data has significant interest.

IV. DISCUSSIONS

We have developed a quantum assisted SOFM and showed a proof-of-concept experimental demonstration that it can be used to solve clustering problems in an unsupervised manner. The procedure of solving such a clustering problem requires calculating the distance many times in iterative way, which is calculated using a hybrid quantum-classical procedure. We introduced an optimized circuit for Hamming distance calculations that can be implemented on currently available quantum com-

puting devices with high fidelity. Our quantum circuit performs the distance-computing component of a classical SOFM algorithm and in this way improves its performance. The complexity of the quantum assisted SOFM scales as $O(LN)$ while the complexity of the fully classical SOFM scales as $O(LMN)$, where N is number of samples, M is number of randomly sampled cluster vectors, and L is number of the shifts of cluster vectors. Due to wide use of classical SOFM in different areas of modern research and technology, this can give opportunities for the use of QASOFM in practical applications in the near term, outperforming classical algorithms. In addition, as our algorithm performs the Hamming distance calculation, it has the potential to enhance any classical algorithm that relies on calculating distances between data entries of vector form. In machine learning, data science, statistics and optimization, distance is a common way of representing similarity, calculating it between large data sets is common procedure and our circuit could potentially enhance other distance-based algorithms as long as exact distance is not required, but when knowledge of nearest vectors is sufficient.

ACKNOWLEDGMENTS

The work was performed as a part of a state task, State Registration No. AAAA-A19-119071190017-7. T.B. is supported by the National Natural Science Foundation of China (62071301); NYU-ECNU Institute of Physics at NYU Shanghai; Shanghai Frontiers Science Center of Artificial Intelligence and Deep Learning; the Joint Physics Research Institute Challenge Grant; the Science and Technology Commission of Shanghai Municipality (19XD1423000, 22ZR1444600); the NYU Shanghai Boost Fund; the China Foreign Experts Program (G2021013002L); the NYU Shanghai Major-Grants Seed Fund; Tamkeen under the NYU Abu Dhabi Research Institute grant CG008; and the SMEC Scientific Research Innovation Project (2023ZKZD55).

CONFLICT OF INTEREST

The authors declare no conflict of interest.

KEYWORDS

quantum self-organizing feature map; quantum machine learning; neural network; quantum unsupervised data clustering; Hamming distance.

[1] LeCun, Y., Bengio, Y. & Hinton, G. Deep learning. *Nature* **521**, 436–444 (2015).

[2] Ghahramani, Z. Probabilistic machine learning and artificial intelligence. *Nature* **521**, 452–459 (2015).

- [3] Schwab, K. *The Fourth Industrial Revolution* (Currency Press, Redfern, New South Wales, 2017).
- [4] Esteva, A. *et al.* A guide to deep learning in healthcare. *Nature Medicine* **25**, 24–29 (2019).
- [5] Tyrsa, V., Carrio, A., Sampedro, C., Rodriguez-Ramos, A. & Campoy, P. A review of deep learning methods and applications for unmanned aerial vehicles. *Journal of Sensors* **2017**, 3296874 (2017).
- [6] Kaggle: Higgs boson machine learning challenge. (2014). URL <https://www.kaggle.com/c/higgs-boson>.
- [7] Radovic, A. *et al.* Machine learning at the energy and intensity frontiers of particle physics. *Nature* **560**, 41–48 (2018).
- [8] Butler, K. T., Davies, D. W., Cartwright, H., Isayev, O. & Walsh, A. Machine learning for molecular and materials science. *Nature* **559**, 547–555 (2018).
- [9] Marcus, G. Deep learning: A critical appraisal. *arXiv:1801.00631* (2018).
- [10] Sze, V., Chen, Y.-H., Yang, T.-J. & Emer, J. S. Efficient processing of deep neural networks: A tutorial and survey. *Proceedings of the IEEE* **105**, 2295–2329 (2017).
- [11] Kourtis, K. *et al.* Compiling neural networks for a computational memory accelerator. *arXiv:2003.04293* (2020).
- [12] Kohonen, T. The self-organizing map. *Proceedings of the IEEE* **78**, 1464–1480 (1990).
- [13] Kohonen, T., Oja, E., Simula, O., Visa, A. & Kangas, J. Engineering applications of the self-organizing map. *Proceedings of the IEEE* **84**, 1358–1384 (1996).
- [14] Kohonen, T. Exploration of very large databases by self-organizing maps. *Proceedings of International Conference on Neural Networks (ICNN'97)* **1**, PL1–PL6 (1997).
- [15] Vilibic, I. *et al.* Self-organizing maps-based ocean currents forecasting system. *Scientific Reports* **6**, 22924 (2016).
- [16] Deboeck, G. & Kohonen, T. *Visual Explorations in Finance* (Springer-Verlag London, Reading, Massachusetts, 1998).
- [17] Doszkocs, T. E., Reggia, J. & Lin, X. Connectionist models and information retrieval. annual review of information science and technology. *ARIST* **25**, 209–260. (1990).
- [18] Jones, F. C. *et al.* The genomic basis of adaptive evolution in threespine sticklebacks. *Nature* **484**, 55–61 (2012).
- [19] Mori, T., Takaoka, H., Yamane, J., Alev, C. & Fujibuchi, W. Novel computational model of gastrula morphogenesis to identify spatial discriminator genes by self-organizing map (som) clustering. *Scientific Reports* **9**, 12597 (2019).
- [20] Corsello, S. M. *et al.* The drug repurposing hub: a next-generation drug library and information resource. *Nature Medicine* **23**, 405–408 (2017).
- [21] Zhu, D., Cao, X., Sun, B. & Luo, C. Biologically inspired self-organizing map applied to task assignment and path planning of an AUV system. *IEEE Transactions on Cognitive and Developmental Systems* **10**, 304–313 (2018).
- [22] Chea, R., Grenouillet, G. & Lek, S. Evidence of water quality degradation in lower mekong basin revealed by self-organizing map. *PLOS ONE* **11**, e0145527 (2016).
- [23] Kiviluoto, K. Topology preservation in self-organizing maps. *Proceedings of International Conference on Neural Networks (ICNN'96)* **1**, 294–299 (1996).
- [24] Dunjko, V. & Briegel, H. J. Machine learning & artificial intelligence in the quantum domain: a review of recent progress. *Reports on Progress in Physics* **81**, 074001 (2018).
- [25] Biamonte, J. *et al.* Quantum machine learning. *Nature* **549**, 195–202 (2017).
- [26] Schuld, M., Sinayskiy, I. & Petruccione, F. An introduction to quantum machine learning. *Contemporary Physics* **56**, 172–185 (2014).
- [27] Carleo, G. *et al.* Machine learning and the physical sciences. *Reviews of Modern Physics* **91**, 045002 (2019).
- [28] Wiebe, N., Braun, D. & Lloyd, S. Quantum algorithm for data fitting. *Physical Review Letters* **109**, 050505 (2012).
- [29] Harrow, A. W., Hassidim, A. & Lloyd, S. Quantum algorithm for linear systems of equations. *Physical Review Letters* **103**, 150502 (2009).
- [30] Childs, A. M., Kothari, R. & Somma, R. D. Quantum algorithm for systems of linear equations with exponentially improved dependence on precision. *SIAM Journal on Computing* **46**, 1920–1950 (2017).
- [31] Lloyd, S., Mohseni, M. & Rebentrost, P. Quantum algorithms for supervised and unsupervised machine learning. *arXiv:1307.0411* (2013).
- [32] Lloyd, S., Mohseni, M. & Rebentrost, P. Quantum principal component analysis. *Nature Physics* **10**, 631–633 (2014).
- [33] Dunjko, V., Taylor, J. M. & Briegel, H. J. Quantum-enhanced machine learning. *Phys. Rev. Lett.* **117**, 130501 (2016).
- [34] Paparo, G. D., Dunjko, V., Makmal, A., Martin-Delgado, M. A. & Briegel, H. J. Quantum speedup for active learning agents. *Phys. Rev. X* **4**, 031002 (2014).
- [35] Rebentrost, P., Mohseni, M. & Lloyd, S. Quantum support vector machine for big data classification. *Physical Review Letters* **113**, 130503 (2014).
- [36] Kamruzzaman, A., Alhwaiti, Y., Leider, A. & Tappert, C. C. Quantum deep learning neural networks. In Arai, K. & Bhatia, R. (eds.) *Knowledge Science, Engineering and Management*, 299–311 (Springer, Cham, 2020).
- [37] Schuld, M., Sinayskiy, I. & Petruccione, F. The quest for a quantum neural network. *Quantum Information Processing* **13**, 2567–2586 (2014).
- [38] Jeswal, S. K. & Chakraverty, S. Recent developments and applications in quantum neural network: A review. *Archives of Computational Methods in Engineering* **26**, 793–807 (2019).
- [39] Broughton, M. *et al.* Tensorflow quantum: A software framework for quantum machine learning. *arXiv:2003.02989* (2020).
- [40] Lewenstein, M. Quantum perceptrons. *Journal of Modern Optics* **41**, 2491–2501 (1994).
- [41] Allcock, J., Hsieh, C.-Y., Kerenidis, I. & Zhang, S. Quantum algorithms for feedforward neural networks. *arXiv:1812.03089* (2018).
- [42] Tacchino, F. *et al.* Quantum implementation of an artificial feed-forward neural network. *arXiv:1912.12486* (2019).
- [43] Cong, I., Choi, S. & Lukin, M. D. Quantum convolutional neural networks. *Nature Physics* **15**, 1273–1278 (2019).
- [44] Liu, J. *et al.* Hybrid quantum-classical convolutional neural networks. *arXiv:1911.02998* (2019).
- [45] Zhao, Z., Pozas-Kerstjens, A., Rebentrost, P. & Wittek, P. Bayesian deep learning on a quantum computer. *Quantum Machine Intelligence* **1**, 41–51 (2019).
- [46] Kerenidis, I. & Luongo, A. Quantum classification of the mnist dataset via slow feature analysis. *arXiv:1805.08837*

- (2018).
- [47] Li, T., Chakrabarti, S. & Wu, X. Sublinear quantum algorithms for training linear and kernel-based classifiers. *arXiv:1904.02276* (2019).
 - [48] Killoran, N. *et al.* Continuous-variable quantum neural networks. *Physical Review Research* **1**, 033063 (2019).
 - [49] Bondarenko, D. & Feldmann, P. Quantum autoencoders to denoise quantum data. *arXiv: 1910.09169* (2019).
 - [50] Dunjko, V., Taylor, J. M. & Briegel, H. J. Advances in quantum reinforcement learning. *2017 IEEE International Conference on Systems, Man, and Cybernetics (SMC)* 282–287 (2017).
 - [51] Nautrup, H. P., Delfosse, N., Dunjko, V., Briegel, H. J. & Friis, N. Optimizing quantum error correction codes with reinforcement learning. *Quantum* **3**, 215 (2019).
 - [52] Fösel, T., Tighineanu, P., Weiss, T. & Marquardt, F. Reinforcement learning with neural networks for quantum feedback. *Physical Review X* **8**, 031084 (2018).
 - [53] Rebentrost, P., Bromley, T. R., Weedbrook, C. & Lloyd, S. Quantum hopfield neural network. *Phys. Rev. A* **98**, 042308 (2018).
 - [54] Purushothaman, G. & Karayiannis, N. Quantum neural networks (QNNs): inherently fuzzy feedforward neural networks. *IEEE Transactions on Neural Networks* **8**, 679–693 (1997).
 - [55] Verdon, G. *et al.* Quantum graph neural networks. *arXiv: 1909.12264* (2019).
 - [56] Cherny, V. V., Byrnes, T. & Pyrkov, A. N. Nontrivial attractors of the perturbed nonlinear schrödinger equation: Applications to associative memory and pattern recognition. *Advanced Quantum Technologies* **2**, 1800087 (2019).
 - [57] Byrnes, T., Koyama, S., Yan, K. & Yamamoto, Y. Neural networks using two-component bose-einstein condensates. *Scientific Reports* **3**, 2531 (2013).
 - [58] Mishra, N. *et al.* Cancer detection using quantum neural networks: A demonstration on a quantum computer. *arXiv: 1911.00504* (2019).
 - [59] Pyrkov, A. N., Byrnes, T. & Cherny, V. V. Solitonic fixed point attractors in the complex ginzburg–landau equation for associative memories. *Symmetry* **12**, 24 (2020).
 - [60] Vinci, W. *et al.* A path towards quantum advantage in training deep generative models with quantum annealers. *arXiv: 1912.02119* (2019).
 - [61] Lu, S., Duan, L.-M. & Deng, D.-L. Quantum adversarial machine learning. *arXiv: 2001.00030* (2019).
 - [62] McClean, J. R., Romero, J., Babbush, R. & Aspuru-Guzik, A. The theory of variational hybrid quantum-classical algorithms. *New Journal of Physics* **18**, 023023 (2016).
 - [63] Arute, F. *et al.* Quantum approximate optimization of non-planar graph problems on a planar superconducting processor. *arXiv: 2004.04197* (2020).
 - [64] Akshay, V., Philathong, H., Morales, M. & Biamonte, J. Reachability deficits in quantum approximate optimization. *Physical Review Letters* **124**, 090504 (2020).
 - [65] Farhi, E., Goldstone, J. & Gutmann, S. A quantum approximate optimization algorithm. *arXiv: 1411.4028* (2014).
 - [66] Farhi, E. & Harrow, A. W. Quantum supremacy through the quantum approximate optimization algorithm. *arXiv: 1602.07674* (2016).
 - [67] Wang, Z., Hadfield, S., Jiang, Z. & Rieffel, E. G. Quantum approximate optimization algorithm for MaxCut: A fermionic view. *Physical Review A* **97**, 022304 (2018).
 - [68] Jiang, Z., Rieffel, E. G. & Wang, Z. Near-optimal quantum circuit for grover’s unstructured search using a transverse field. *Physical Review A* **95**, 062317 (2017).
 - [69] Huang, C. *et al.* Alibaba cloud quantum development platform: Applications to quantum algorithm design. *arXiv: 1909.02559* (2019).
 - [70] Wecker, D., Hastings, M. B. & Troyer, M. Training a quantum optimizer. *Physical Review A* **94**, 022309 (2016).
 - [71] Pagano, G. *et al.* Quantum approximate optimization of the long-range ising model with a trapped-ion quantum simulator. *arxiv: 1906.02700* (2019).
 - [72] Byrnes, T., Forster, G. & Tessler, L. Generalized grover’s algorithm for multiple phase inversion states. *Physical Review Letters* **120**, 060501 (2018).
 - [73] Kandala, A. *et al.* Hardware-efficient variational quantum eigensolver for small molecules and quantum magnets. *Nature* **549**, 242–246 (2017).
 - [74] Aspuru-Guzik, A. Simulated quantum computation of molecular energies. *Science* **309**, 1704–1707 (2005).
 - [75] Lanyon, B. P. *et al.* Towards quantum chemistry on a quantum computer. *Nature Chemistry* **2**, 106–111 (2010).
 - [76] Peruzzo, A. *et al.* A variational eigenvalue solver on a photonic quantum processor. *Nature Communications* **5**, 4213 (2014).
 - [77] Preskill, J. Quantum computing in the NISQ era and beyond. *Quantum* **2**, 79 (2018).
 - [78] IBM Quantum Experience. URL <https://www.ibm.com/quantum-computing/>.
 - [79] Solan, Z. & Ruppin, E. Similarity in perception: A window to brain organization. *Journal of Cognitive Neuroscience* **13**, 18–30 (2001).
 - [80] Appiah, K. *et al.* A binary self-organizing map and its FPGA implementation. *2009 International Joint Conference on Neural Networks* 164–171 (2009).
 - [81] Santana, A., Morais, A. & Quiles, M. G. An alternative approach for binary and categorical self-organizing maps. *2017 International Joint Conference on Neural Networks (IJCNN)* 2604–2610 (2017).
 - [82] Trugenberger, C. A. Probabilistic quantum memories. *Physical Review Letters* **87**, 067901 (2001).
 - [83] Rui, W., Xing, K. & Jia, Y. Bowl: Bag of word clusters text representation using word embeddings. In Lehner, F. & Fteimi, N. (eds.) *Knowledge Science, Engineering and Management*, 3–14 (Springer International Publishing, Cham, 2016).
 - [84] Asselmeyer-Maluga, Torsten. Quantum computing and the brain: quantum nets, dessins d’enfants and neural networks. *EPJ Web Conf.* **198**, 14 (2019).
 - [85] Daskin, A. A simple quantum neural net with a periodic activation function. *2018 IEEE International Conference on Systems, Man, and Cybernetics* 2887–2891 (2018).
 - [86] Nguyen, N. T. & Kenyon, G. T. Image classification using quantum inference on the d-wave 2x. *2018 IEEE International Conference on Rebooting Computing* 2887–2891 (2018).
 - [87] Cheng, Y. *et al.* Targeting epigenetic regulators for cancer therapy: mechanisms and advances in clinical trials. *Signal Transduction and Targeted Therapy* **4**, 62 (2019).
 - [88] Steck, S. E. & Murphy, E. A. Dietary patterns and cancer risk. *Nature Reviews Cancer* **20**, 125–138 (2020).
 - [89] Ghasemi, S. Cancer’s epigenetic drugs: where are they in the cancer medicines? *The Pharmacogenomics Journal*

- 20**, 1473–1150 (2019).
- [90] Wang, X. *et al.* Circular rna ttn acts as a mir-432 sponge to facilitate proliferation and differentiation of myoblasts via the igf2/pi3k/akt signaling pathway. *Molecular Therapy - Nucleic Acids* **18**, 966 – 980 (2019).
 - [91] Zhou, B. *et al.* Eukaryotic elongation factor 2 is involved in the anticoccidial action of diclazuril in the second-generation merozoites of eimeria tenella. *Veterinary Parasitology* **276**, 108991 (2019).
 - [92] Jiao, L. *et al.* Correlation of CpG methylation of the pdcd1 gene with PD-1 expression on CD8 + t cells and medical laboratory indicators in chronic hepatitis b infection. *The Journal of Gene Medicine* **22**, e3148 (2020).
 - [93] McTear, M., Callejas, Z. & Griol, D. *The Conversational Interface* (Springer International Publishing, 2016).
 - [94] Abraham, H. *et al.* Qiskit: An open-source framework for quantum computing (2019).